Atmospheric Correction at AERONET Locations: A New Science and Validation Data Set

Yujie Wang[1,2], Alexei Lyapustin[1,2], Jeffery L. Privette[3], Jeffery T. Morisette[2], Brent Holben[2]

[1]GEST center, University of Maryland Baltimore county, Catonsville, MD 21228
[2]NASA Goddard Space Flight Center, Greenbelt, MD 20771
[3]NCDC, NOAA Satellite and Information Service, Asheville, NC 28801

Abstract

This paper describes an AERONET-based Surface Reflectance Validation Network (ASRVN) and its dataset of spectral surface bidirectional reflectance and albedo based on MODIS TERRA and AQUA data. The ASRVN is an operational data collection and processing system. It receives 50×50 km^2 subsets of MODIS L1B data from MODAPS and AERONET aerosol and water vapor information. Then it performs an accurate atmospheric correction for about 100 AERONET sites based on accurate radiative transfer theory with high quality control of the input data. The ASRVN processing software consists of L1B data gridding algorithm, a new cloud mask algorithm based on a time series analysis, and an atmospheric correction algorithm. The atmospheric correction is achieved by fitting the MODIS top of atmosphere measurements, accumulated for 16-day interval, with theoretical reflectance parameterized in terms of coefficients of the LSRT BRF model. The ASRVN takes several steps to ensure high quality of results: 1) cloud mask algorithm filters opaque clouds; 2) an aerosol filter has been developed to filter residual semi-transparent and sub-pixel clouds, as well as cases with high inhomogeneity of aerosols in the processing area; 3) imposing requirement of consistency of the new solution with previously retrieved BRF and albedo; 4) rapid adjustment of the 16-day retrieval to the surface changes using the last day of measurements; and 5) development of seasonal back-up spectral BRF database to increase data coverage. The ASRVN provides a gapless or near-gapless coverage for the processing area. The gaps, caused by clouds, are filled most naturally with the latest solution for a given pixels. The ASRVN products include three parameters of LSRT model (k^L, k^G, k^V), surface albedo, NBRF (a normalized BRF computed for a standard viewing geometry, VZA=0^o, SZA=45^o), and IBRF (instantaneous, or one angle, BRF value derived from the last day of MODIS measurement for specific viewing geometry) for MODIS 500m bands 1-7. The results are produced daily at resolution of 1 km in gridded format. We also provide cloud mask, quality flag and a browse bitmap image. The new dataset can be used for a wide range of applications including validation analysis and science research.

1. Introduction

Validation of the moderate resolution (~1km) surface reflectance products, including spectral bi-directional reflectance factor (BRF), albedo, vegetation indices and others, is an important component of the Earth Observing System (EOS) [1] and the National Polar Orbiting Environmental Satellite System programs. Its goal is to establish the accuracy of environmental data products on regional and global scales for a broad range of atmospheric and surface conditions. The EOS program has developed a multi-level strategy with a strong field campaign component [2-5]. The field measurements required for *direct* validation analysis provide a detailed and comprehensive look at the local properties, but they usually involve significant resources, are subject to weather uncertainties, and are strongly limited in temporal and spatial coverage. Due to these constraints, recent validation efforts have proposed that product accuracy

assessment should also utilized a globally representative sample of sites to complement the direct validation sites [6]. This concept has been endorsed by the Committee on Earth Observing Satellites (CEOS) as the Bench-mark Land Multisite Analysis and Intercomparision of Products (BELMANIP) [7].

In this paper, we present an alternative validation approach for moderate resolution global surface reflectance products over Aerosol Robotic Network (AERONET) sunphotometer sites [8]. The idea is to collect the best ancillary information on atmospheric aerosol and water vapor, and perform an independent atmospheric correction of satellite measurements based on accurate radiative transfer theory with high quality control of the input data and results. In the past several years, we have implemented this idea in the AERONET-based Surface Reflectance Validation Network (ASRVN) which is an automated data collection and processing system residing on a dedicated workstation. ASRVN operationally receives the satellite sensors' L1B data (currently MODIS TERRA and AQUA from the Goddard's MODAPS and MISR from Langley's DAAC) and aerosol and water vapor information from the AERONET server. After a successful test of data integrity and completeness, ASRVN automatically performs rigorous atmospheric correction on each sensor's data, creating a sensor-specific record of spectral BRF, albedo and derivative products (e.g., vegetation index) over more than 100 AERONET sites globally. For each site, products are stored in a gridded format at 1 km resolution for an area of 50x50 km^2 for MODIS and 32x32 km^2 for MISR. Currently, the ASRVN dataset contains 8 years of MODIS TERRA data (since 2000), and 4 years of MODIS AQUA data. The AQUA dataset will be completed together with MODIS Collection 5 land re-processing, which produces the MODIS AQUA subsets for the ASRVN.

Many of the ideas implemented in ASRVN originated in the MODIS BRDF/Albedo algorithm [9] similarly based on the time series analysis within 16-day intervals. In this paper, we will be using the term BRF (bi-directional reflectance factor) rather than more commonly used BRDF (bi-directional reflectance distribution function), which is just a factor of π smaller than BRF.

The ASRVN algorithm for MISR data was presented previously [10]. This paper describes processing algorithm for MODIS measurements (sections 2-3). Examples of ASRVN dataset are given in section 4. The paper concludes with a summary.

2. ASRVN Infrastructure

The BRF retrievals from MODIS data use several clear-skies measurements acquired on successive observations of the same area under different viewing geometries. The *ASRVN* processing starts by gridding the latest MODIS swath data (generated operationally over each AERONET site by the MODAPS production system) and placing the resulting *ASRVN Tile* in a 16-day processing Queue, which implements a sliding temporal window algorithm. Note the *ASRVN Tile* is distinct from the much larger MODIS Land Team's production Tile. Next, it finds a relevant AERONET aerosol and water vapor record and computes radiative transfer functions required for atmospheric correction. After ensuring the quality of input data by filtering clouds and spatially variable aerosols, the *ASRVN* algorithm performs atmospheric correction and checks the quality of the final solution. The next three sections will describe pre-processing steps preceding the BRF retrieval.

2.1 Ancillary Data

AERONET sunphotometers sample the direct solar radiation each 15 minutes, and sample diffuse sky radiance over a wide range of angles every 60 minutes during the daytime. AERONET's automated processing system generates AOT and column water vapor from the direct solar measurements. Typical AOT uncertainty for a field instrument is 0.01-0.02 and is spectrally dependent. The inversion algorithm [11] uses almucantar sky measurements to retrieve aerosol microphysical properties (particle size distribution and refractive index) and concentration. AERONET applies several tests to ensure reliability of retrievals, such as SZA $\geq$ 45^{o}, $AOT_{0.44} \geq 0.4$, and that there were at least 21 independent angles used in each inversion. The tests analyze sensitivity of retrievals to the single scattering albedo, and to the phase function at large scattering angles. These quality assurance tests significantly reduce the number of complete aerosol characterization records, as compared to the number of AOT records.

The *ASRVN* algorithm starts with the selection of AERONET aerosol optical thickness and column water vapor values within 30 minutes of satellite overpass. If these conditions are met, the algorithm selects the inversion record with aerosol microphysical parameters and size distribution within 2 hours of overpass. Otherwise, it uses an aerosol climatology model for a given location derived from multi-year AERONET statistics of reliable retrievals [12]. Because full AERONET inversions are less accurate when aerosol concentration is low, the climatology background aerosol model is always used in our algorithm for clear atmospheric conditions (currently defined as $AOT_{0.44} \leq 0.3$). Our testing demonstrates that the aerosol climatology significantly improves the stability of the time series of derived surface albedo.

Following the selection of aerosol parameters, *ASRVN* algorithm calculates the aerosol optical thickness (AOT_{MIE}), single scattering albedo, and scattering phase function using a look-up table approach [13]. Depending on AERONET sphericity index, either a spherical (Mie) aerosol model or a model of spheroids is used. The above calculations provide the spectral dependence of extinction (AOT_{MIE}) in the MODIS wavelengths. However, the AOT from direct solar measurements may differ from AOT_{MIE} for a number of reasons, from the time difference between inversion and direct AOT measurement to uncertainties associated with the AERONET inversion algorithm [14] etc. For this reason, AOT_{MIE} is further scaled by fitting it to the measured AOT at three AERONET wavelengths (0.44, 0.67, and 0.87 μm). Once aerosol optical parameters are defined, the radiative transfer model SHARM [15] calculates the required radiative transfer functions for the specific water vapor and spectral response functions of MODIS TERRA or AQUA instrument using the Interpolation and Profile Correction (IPC) method [16].

2.2 Implementation of Time Series Processing

To execute time series processing (sliding window algorithm), *ASRVN* first grids MODIS level 1B (L1B) calibrated and geolocated data to a regular 1 km grid. We use the MODIS land gridding algorithm [17] with minor modifications that allow us to better preserve the angular anisotropy of signals in the gridded data when measured reflectance is high, for example over snow, thick clouds or water with glint. Next, gridded MODIS data (*Tiles*) are placed in the processing Queue, which can hold up to 16 days of successive measurements. The *ASRVN* processing uses both individual grid cells, also called pixels below, and fixed-size (25×25 km^2) areas, or blocks, required by the cloud mask algorithm. In order to organize such processing, we developed a framework of C++ classes and structures (algorithm-specific Containers). The class

functions are designed to handle processing in the various time-space scales, for example at the pixel- or block-level, and for a single (last) day of measurements or all available days in the Queue, or for a subset of days which satisfy certain requirements (filters). The data storage in the Queue is efficiently organized using pointers, which avoids physically moving the previous data in memory when the new data arrive.

The structure of the Queue is shown schematically in Figure 1. For every day of observations, MODIS measurements are stored as Layers for reflective bands 1-7 and thermal band 32, all of which are required by the CM algorithm. Besides storing gridded MODIS data (*Tiles*), the Queue has a dedicated memory (Q-memory) which accumulates ancillary information about every block and pixel of the surface for the cloud mask algorithm (*Refcm* data structure). It also keeps information related to the history of previous retrievals, such as surface BRF parameters and albedo. Given the daily rate of MODIS observations, the land surface is relatively static over most 16-day periods. Therefore, knowledge of the previous surface state significantly enhances both the accuracy of the cloud detection and the quality of atmospheric correction by imposing a requirement of consistency of the time series of BRF and albedo.

2.3 Data Quality Control: Cloud Mask and Aerosol Filter

From the start, *ASRVN* was designed to work with a multipixel area rather than a single pixel centered at an AERONET location in order to provide optimal visual control over the input and output results. Visual analysis of RGB images is superior for complex data quality assessment and troubleshooting situations which is rarely achievable with a pixel- (or point-) level analysis.

Although AERONET produces an internal cloud mask [18], it is not sufficient for atmospheric correction over the 50×50 km^2 processing area. For example, the sunphotometer may provide AOT measurements from a direct sun view through a gap in the clouds. Usually, the sunphotometer's time of measurement differs from satellite overpass time, in which case changes in cloudiness may have occurred. For these reasons, we implemented a new *MAIAC* Cloud Mask algorithm [19] as part of the *ASRVN* processing. This algorithm uses the time series analysis and an image-based rather than pixel-based analysis. It explicitly addresses the problem of cloud searching by identifying a clear-skies comparison target. *MAIAC* CM constructs the reference clear-skies image of the surface and stores it along with other ancillary information about reflectance and brightness temperature for every surface block (25×25 km^2). This ancillary information, required for cloud detection, is continuously updated with the latest cloud-free measurements. This allows CM to dynamically adjust to gradual (seasonal) and rapid surface changes caused by snowfall, fires, floods, etc. The CM algorithm is enhanced by an internal dynamic land-water-snow classification, which allows processing flexibility over varying surface types.

Our experience with MODIS data processing dictated the need for additional data screening. This is required when aerosols have significant spatial variation and a single AERONET AOT value does not represent the full processing area, as well as in cases of undetected, usually semi-transparent and sub-pixel, clouds. This screening was implemented through an "aerosol filter". Using the known surface BRF from previous retrievals, the algorithm computes the pixel-level AOT in the blue band from the latest MODIS measurements. The AOT retrieval is a fast algorithm based on a look-up table pre-calculated for a standard continental aerosol model. The computed AOT is used solely to assess spatial homogeneity of aerosols over

the processing area, and to find deviations, which usually indicate previously undetected clouds and sometimes spatially varying aerosols. Specifically, the algorithm generates an AOT histogram from the non-cloudy pixels, filters the highest 20% values as possibly cloudy, and finds the average value (AOT_{av}) for the remaining 80% of the pixels. This AOT_{av} is assumed to represent the average clear-skies aerosol loading over the processing area, which should correspond to the AERONET AOT. The AOT_{av} is used next to further filter "suspicious" (contaminated) data as follows: if the atmosphere is clear ($AOT_{av}<0.25$), then the algorithm filters only pixels with the high AOT values exceeding the average by 0.15 or more. This threshold was determined through trial and error. Otherwise, it filters the high and low values symmetrically if the difference with AOT_{av} exceeds ±0.15. This relatively simple technique allows us to filter sub-pixel clouds, contrails and other forms of thin cirrus and semi-transparent clouds. With the introduction of this additional filter, we witnessed a dramatic enhancement in the quality of the *ASRVN* atmospheric correction.

Figure 2 shows examples of the cloud mask algorithm and aerosol filter for the Goddard Space Flight Center (Greenbelt, Maryland, USA) site. It shows that the CM algorithm captures most of the opaque clouds, whereas the aerosol filter captured additional sub-pixel and semi-transparent clouds and cases of spatially variable aerosols. The example at the bottom of Figure 2 also shows the detection of cloud shadows by *MAIAC* CM algorithm. Shadows are detected with a simple threshold algorithm which compares the latest MODIS measurement (ρ^{meas}) with predicted reflectance from the previously retrieved BRF model parameters (ρ^{pred}):

$$\text{IF } \rho^{meas} < \rho^{pred} - 0.12 \Rightarrow \textit{CLOUD\_SHADOW}.$$

Here, we use MODIS wavelength 1.24 μm (band 5) which experiences minimal atmospheric distortions and is usually bright over land so the change of reflectance due to cloud shadow can be easily detected well above the sensor noise level.

3. Atmospheric Correction

Once the cloud mask, enhanced by aerosol filter, is applied, the *ASRVN* algorithm filters the time series of MODIS measurements for every single pixel, and places the remaining good data in a "container". The container stores measurements along with computed RT functions for the cloud-free days of the Queue. If the number of good measurements exceeds 3 for a given pixel (see section 3.2), then the coefficients of Li-Sparse Ross-Thick (LSRT) BRF model [20] are computed. The LSRT model is used in the MODIS BRDF/albedo algorithm [9].

3.1 Inversion for LSRT Coefficients

In the operational MODIS land processing system, the BRF is determined in two steps: first, the atmospheric correction algorithm derives surface reflectance for a given observation geometry using a Lambertian approximation [21]. Next, three LSRT coefficients are retrieved from the time series of surface reflectance accumulated for a 16-day period [9]. The Lambertian assumption simplifies the atmospheric correction but imparts biases which depend on observation geometry and atmospheric opacity. Tests show that the Lambertian assumption leads to a more Lambertian BRF shape while the true BRF is more anisotropic [22].

The *ASRVN* algorithm derives surface LSRT coefficients directly by fitting the radiative transfer solution to the measured TOA reflectance accumulated over a 4-16 day period. The inversion is based on a high accuracy semi-analytical Green's function solution [23, 24], which

in combination with LSRT BRF model provides an explicit parameterization of TOA reflectance in terms of the surface BRF model parameters $\vec{K}=\{k^L,\ k^G,\ k^V\}^T$. According to the derivation provided in the Appendix, the TOA reflectance can be expressed as:

$$R(\mu_0,\mu,\varphi)=R^D(\mu_0,\mu,\varphi)+k^L F^L(\mu_0,\mu)+k^G F^G(\mu_0,\mu,\varphi)+k^V F^V(\mu_0,\mu,\varphi)+R^{nl}(\mu_0,\mu), \quad (1)$$

where R^D is the atmospheric (path) reflectance, and R^{nl} is a small non-linear term proportional to the product of surface albedo and spherical albedo of the atmosphere ($R^{nl}\propto qc_0$). Functions F^L, F^V and F^G depend on geometry and atmospheric conditions. They are weakly non-linear in *k*-coefficients through the multiple reflection factor $\alpha=(1-qc_0)^{-1}$.

The quasi-linear form of equation (1) leads to a very efficient iterative minimization algorithm:

$$RMSE=\sum_j (r_j^{(n)}-F_j^L k^{L(n)}-F_j^V k^{V(n)}-F_j^G k^{G(n)})^2=\min_{\{\vec{K}\}},\ r^{(n)}=R-R^D-R^{nl(n-1)}, \quad (2)$$

where index *j* denotes measurements for different days, and *n* is the iteration number. Equation (2) provides an explicit least-squares solution for the kernel weights. In matrix form, the solution is written as:

$$\vec{K}^{(n)}=A^{-1}\vec{b}^{(n)}, \quad (3)$$

where

$$A=\begin{bmatrix} \sum (F_j^L)^2 & \sum_j F_j^G F_j^L & \sum_j F_j^V F_j^L \\ \sum_j F_j^G F_j^L & \sum_j (F_j^G)^2 & \sum_j F_j^V F_j^G \\ \sum_j F_j^V F_j^L & \sum_j F_j^V F_j^G & \sum_j (F_j^V)^2 \end{bmatrix},\ \vec{b}^{(n)}=\begin{bmatrix} \sum_j r_j^{(n)} F_j^L \\ \sum_j r_j^{(n)} F_j^G \\ \sum_j r_j^{(n)} F_j^V \end{bmatrix}.$$

In the first iteration, the small non-linear term is set to zero, $R_j^{nl(0)}=0$, and the multiple reflection factor α (see Appendix) is set to one, $\alpha^{(0)}=1$. These parameters are updated once after the BRF coefficients are calculated in the first iteration. Except for snow-covered surfaces, the problem converges with high accuracy in two iterations because the non-linear terms are small. Currently, the ASRVN algorithm does not make retrievals over snow.

The described algorithm has a high computational efficiency. Compared to the radiative transfer computations, the time required to evaluate functions F^m (*m*=*L*, *V*, *G*) and R^{nl} is negligible. The integrals required for these functions (see Appendix) need to be calculated only once regardless of the number of iterations. Finally, small variations of the viewing geometry across the processing area are neglected and the RT calculation is done once per observation using the geometry of the central pixel.

3.2 Solution Selection and Update

Although the LSRT model leads to an efficient BRF retrieval algorithm, there are several caveats associated with this model. The LSRT kernels are not orthogonal, are not positive-only functions, and are normalized in a somewhat arbitrary fashion that is not linked to radiative transfer theory. These factors reduce the stability and uniqueness of the solutions, such that small

perturbations in measurements may lead to significantly different solutions. The high goodness-of-fit at the measurement angles does not guarantee the correct shape of the retrieved BRF, and may result in negative BRF values at other angles. The albedo, being an integral function of BRF, is especially sensitive to an incorrect BRF shape. For these reasons, we developed several tests to remove unrealistic solutions.

The initial validation of the solution (see Figure 3) checks that the maximal difference over all days of the Queue between measured and computed TOA reflectance does not exceed a specified threshold ($\left|R^{Meas} - R^{LSRT}\right|$>0.08). The day (measurement) with the highest deviation is excluded from the Queue and the inversion is repeated. If the number of measurements goes below three after the exclusion, no retrieval will be made for this pixel.

If a solution provides a good agreement with measurements for all days, the algorithm verifies that values of the direct-beam albedo (q) at SZA=15^o, 45^o, 60^o are positive. Finally, the new solution must be consistent with the previous solution: $\left|q(45^o) - q^{Prev}(45^o)\right|$<$\Delta(\lambda)$, where Δ is the band-dependent threshold currently equal to 0.04 (blue), 0.05 (green and red), and 0.1 (NIR and shortwave infrared bands). Consistency of the time series of BRF and albedo is characterized by a *status* index. Initially, the confidence in the solution is low (*status*=0). Each time the new retrieval agrees with the previous retrieval, *status* increases by 1. When *status*≥3, the retrieval is considered reliable.

When the new solution is validated, the coefficients of the BRF model and direct-beam albedo $q(45^o)$, stored in the Q-memory, are updated. The update is done with relaxation, designed to mitigate random noise of retrievals:

$$\vec{K}_\lambda^{New} = (\vec{K}_\lambda^{New} + \vec{K}_\lambda^{Prev})/2. \quad (4)$$

This method of update increases the quality of the BRF and albedo product when the surface is relatively stable, but it delays the response of the solution to surface changes.

Often, the solution for some pixels or the full area cannot be produced because of lack of clear-skies measurements. In these cases, we assume that the surface does not change and we fill-in data gaps with the previous solution for up to a 32-day period. In most cases, this assumption of a stable surface is reasonable. The gap-filled pixel is marked as "Extended" in the quality assurance (QA) value, with parameter QA.*nDelay* giving the number of days since the last update (see section 3.6).

3.3 *ASRVN* Products

The *ASRVN* computes two main products at 1 km resolution for seven 500m MODIS bands, the set of BRF coefficients, and the surface albedo. The albedo is defined by Equation (A-5a) as a ratio of surface-reflected to incident radiative fluxes. Thus, it represents a true albedo at a given solar zenith angle in ambient atmospheric conditions, the value, which can be directly compared to ground-based measurements.

ASRVN also computes several derivative products useful for science data analysis and validation:

1) *NBRF* - a BRF Normalized to the common geometry of nadir view and SZA = 45^o. This product is analogous to MODIS NBAR (nadir BRF-adjusted reflectance) product (part of

the MOD43 standard product suite). With the geometry variations removed, the time series of *NBRF* is useful for studying vegetation phenology, performing surface classification, etc.

2) *IBRF* – an instantaneous (or one-angle) BRF value for the specific viewing geometry of the last day of observations. In essence, *IBRF* is a reflectance which would be measured if the atmosphere were absent. This product is calculated from the latest MODIS measurement assuming that the shape of BRF, known from previous retrievals, didn't change. To illustrate computation of *IBRF*, we re-write equation (1) for the measured TOA reflectance as follows:

$$R(\mu_0, \mu, \varphi) = R^D(\mu_0, \mu, \varphi) + bR^{Surf}(\mu_0, \mu, \varphi), \quad (5)$$

where R^{Surf} combines all surface related terms and can be calculated using the previous solution for BRF (BRF_λ) and AERONET aerosol information. b is spectrally-dependent scaling factor. Then,

$$IBRF_\lambda(\mu_0, \mu, \varphi) = b_\lambda BRF_\lambda(\mu_0, \mu, \varphi). \quad (6)$$

This algorithm (Equation 6) will be referred to as scaling. This description was given for the purpose of illustration. In reality, R^{Surf} is a non-linear function so computing parameter b_λ and *IBRF* is done accurately using the formulas given in the Appendix.

The algorithm computing scaling coefficient (and *IBRF*) is shown in Figure 3 on the right. First, the algorithm filters measurements which differ from the theoretically predicted TOA reflectance based on the previous solution (R_Q^{LSRT}) by more than factor of $\Delta(\lambda)$. Then, the scaling coefficients are computed, and the consistency requirement is verified as: $0.8<b_\lambda<1.2$. If all conditions are satisfied and the *status* of the pixel is high (*status*≥3), then the LSRT BRF parameters of the pixel stored in the Q-memory are updated with the scaled solution:

$$\vec{K}_\lambda^{New} = \frac{b_\lambda + 1}{2} \vec{K}_\lambda^{Prev}. \quad (7)$$

Based on its definition, *IBRF* is well suited for validation of surface reflectance product of the operational atmospheric correction algorithm (standard product MOD09 [21]).

The cloud mask, the RGB browse images for MODIS TOA reflectance and for the ASRVN NBRF and IBRF, and the QA flag, are also standard parts of the ASRVN product suite. The products are saved in HDF-EOS format files, which can automatically keep geolocation information and allow data to be ported to virtually any computer platform, regardless of the byte order of the native platform. A list of the ASRVN products and their MODIS products counterparts are given in Table 1, and the definition of the cloud mask values is provided in Table 2.

3.4 Update in Case of Rapid Surface Change

Time series processing is intrinsically controversial when a surface changes rapidly. Since inversions are generally ill-posed problems, one desires all available cloud-free measurements and a maximal time window in order to reduce the *RMSE.* This approach, which reduces the impact of noise in the data (including that of gridding and of residual clouds) and which ensures a more robust BRF shape, is best when the surface is stable throughout the accumulation period. For example, this is the case for natural ecosystems in mid-latitudinal summers. In contrast, detecting and tracking surface changes like spring green-up, agricultural

harvesting or fall senescence requires the least possible number of days in the inversion Queue. Such retrievals may have a considerable amount of spatial and spectral noise. Indeed, it is difficult to assess the reliability of solutions when the surface reflectance is changing rapidly or abruptly, especially given the possibility of data gaps due to clouds.

While the response of the 16-day solution may be delayed, the *IBRF* tracks spectral changes immediately. The update of Q-memory with the latest measurements by equation (7) was found to significantly accelerate the response of LSRT coefficients ($\vec{K}_\lambda$), and hence of the NBRF, to changing surface conditions. Yet, in some cases we found this insufficient. To amend results in these cases, we added a separate update of the Q-solution with *IBRF* based on change detection. This path is shown at the bottom of Figure 3. Usually, seasonal surface changes related to the vegetation cycle are accompanied by a correlative change in the red-NIR bands, for example, a simultaneous decrease of red and increase of NIR reflectance during green-up, and the opposite changes during fall senescence and defoliation for broadleaf forests. In our case, the change detection is based on the top-of-canopy Normalized Difference Vegetation Index (NDVI). The scene-average NDVI, normalized to a standard viewing geometry of NBRF, is calculated using the *IBRF* ($NDVI^I$). It is compared to the scene-average $NDVI^Q$ calculated using the NBRF stored in the Q-memory (previous reliable solution). A change is defined as when the difference between the two values exceeds ±0.01. At the same time, the red and NIR reflectance should change accordingly. For example, the following set of rules defines the change during spring green-up:

$$NDVI^I - NDVI^Q > 0.01,\ \rho^I_{\mathrm{Red}} - \rho^Q_{\mathrm{Red}} < 0,\ \rho^I_{NIR} - \rho^Q_{NIR} > 0\,.$$

Such an approach filters fluctuations in NDVI caused by factors unrelated to the vegetation signal, such as residual cloudiness or undetected cloud shadows. Once the change is detected, the Q-memory is updated using Eq. (7). Empirically, we found that this approach, which is responsible for 10-15% of all updates, performs robustly at different global AERONET locations, for example in North America, Eurasia, or Africa.

The NBRF and albedo are also updated following an update of $\vec{K}_\lambda$ coefficients. This method, which requires only one last day of measurements when the BRF shape is reliably known, is similar to the scheme used in the MODIS BRDF/albedo algorithm [9] and its reliability has been tested with a global composite AVHRR data set [25]. An advantage of this strategy is that once initialized, the algorithm provides near gapless coverage, and a continuous time series of NBRF and albedo.

Besides providing a faster response to surface change, our update strategy assures fast removal of retrieval artifacts, mainly residual clouds, which is the most common problem.

3.5 Seasonal Ancillary BRF

When no reliable retrievals are made during the past 32 days, which is usually caused by high cloudiness, the previous retrievals are considered unreliable and the Q-memory is refreshed with fill values. After that, it may take the algorithm a considerable amount of time to re-initialize, during which time no results will be produced. To remedy this situation, we developed the historical 1 km resolution BRF database from 5 year retrievals, which is used for BRF-scaling when the Q-memory is being refreshed. The database contains one set of spectral K-coefficients for every pixel for each of the four calendar seasons. Initially, the database is built

from a multi-year run of ASRVN. The images used for averaging, are selected according to the standard deviation of NBRF (σ_{NBRF}) computed for the processing area. Empirically, we found that with our data quality assurance, the top 20% of images with the highest standard deviation usually contain artifacts from residual clouds or unreliable BRF solutions, whereas the remaining 80% of retrievals have a good quality. Thus, for each site and every season, we first generate the histogram of σ_{NBRF}, find the 80% threshold, and average the images with σ-values lower than the threshold.

Once the seasonal BRF database is created, it is supported by an offline background algorithm which updates it with the latest good quality solution.

3.6 Quality Assurance (QA) Flag

For each execution, the algorithm creates a pixel-level QA flag to indicate the overall quality and the internal processing path. The QA information consists of 16-bit compound bit-fields, as summarized in Table 3.

The *QA.overall* field indicates the overall data quality. Four values are possible:

1) Good. This means that the *status* of solution is 3 or greater. In other words, at least three of the last LSRT retrievals agreed, and the calculated IBRF was found to be consistent with the model predictions;
2) Acceptable. In this level, the *status* is not high (<=2), but the calculated IBRF agrees with the model prediction. This case may represent a good solution where only a few retrievals are available because of a gap in AERONET data or clouds;
3) Extended. In this case, either the solution was not produced because of a lack of clear-sky measurements, or the calculated IBRF did not agree well with the model prediction. In this case, the previous reliable solution for a given pixel is used to fill-in the values of the LSRT coefficients and NBRF. The IBRF in this case is not produced;
4) Not created. This usually happens at the beginning of processing when the Q-memory is not yet initialized.

The field *QA.nDelay* gives the number of days since the last update of the Q-memory. If *QA.nDelay* =0, then this pixel contains the most recent retrieval. If the Q-memory was not updated for 32 or more days, the information for a given pixel will be overwritten with the fill value. If the solution is calculated with (Eq. 7), the *QA.scale* field will be set to 1 to indicate that the solution is "scaled" from the previous reliable retrieval. The value of the cloud mask for a given pixel is stored in the field *QA.cloud*. We also mask pixels which are adjacent to cloudy pixels, where greater errors in the atmospheric correction are expected. For such pixels, the *QA.adjCloud* field is set to 1 (the default value is 0).

4. Processing Examples

We selected three AERONET sites, Goddard Space Flight Center (GSFC, 38.9925^{o}N, 76.84^o W), Mongu, Zambia (15.25^{o}S, 23.15^{o}E) and Solar Village, Saudi Arabia (24.91^{o}N, 46.41^{o}E) to illustrate the ASRVN dataset. These sites have very different land cover types, atmospheric conditions and seasonal variations.

- The GSFC site is located in a northern suburb of Washington, DC. It is a mixture of urban residential area, small deciduous broad leaf forest stands and small patches of agriculture cropland.
- The Mongu site is located on the eastern side of Zambezi River in western Zambia. The western part of the area is a floodplain mostly covered with grasses, and the eastern part is mainly a sandy soil with sparse vegetation. Significant biomass burning happens in August and September. In the wet season (November-March), this area has frequent cloud cover.
- The Solar Village site is a desert area, with very stable surface conditions. The dominant aerosol source is dust.

Below, we provide several examples to demonstrate *ASRVN* products, data quality and potential applications. For this study, we used MODAPS Collection 5 data exclusively.

4.1 NBRF time series

The NBRF product has been corrected for both atmospheric effects and variations of view geometry. Thus, NBRF variations should be closely related to changes in surface conditions. Figure 4 shows the seasonal dynamics of the NBRF images for the three sites. The "true color" images are composed with equal weights from the red, green and blue spectral bands. The columns show the gridded TOA reflectance, NBRF and the new cloud mask (the CM legend is given in the figure's caption). Seasonal changes are easy to observe in the first two columns. The vegetative cover reaches a maximum in July-August for the GSFC site, whereas at Mongu, green vegetation is most abundant in January-February, at the height of the wet season. Surface reflectance at the Solar Village site exhibits little variation throughout the year as is expected for a desert surface with little vegetation.

To demonstrate the algorithm's performance with different surface types, we selected two pixels for GSFC that differ in the amount of vegetation – a "green" pixel [pixel (16, 36)] in the middle of a small deciduous forest stand to the north-east of the center, and a relatively bright "urban" pixel [pixel (46, 3)] representing a typical residential area with mixed vegetation at the lower-left corner of the image.. For comparison, we also selected a "bright" pixel [pixel (10, 20)] in the desert region of Solar Village. The locations of these pixels are indicated by color circles in Fig. 4. The NBRF time series for these pixels are shown in Fig. 5. For the "green" pixel, the NBRF in the NIR band increases rapidly during springtime, while the red, green, and blue reflectances decrease. There is an interesting dynamic between the red and green signals. In the early spring, reflectance in the red channel is greater than in the green channel. This is typical of most soils. With the spring green-up, the red band reflectance decreases significantly due to chlorophyll absorption while the change in the green band reflectance is much smaller. During the autumn season, the bands change in the reverse direction as expected for senescing vegetation (Fig. 5a). The "urban" pixel shows a similar temporal trend, but with much smaller amplitude (Fig. 5b). The time series of the "bright" pixel at Solar Village does not show much variation throughout the year. The NBRF of band 7 and the NIR, red, green and blue bands remains around 0.5, 0.42, 0.35, 0.24, and 0.14 respectively . The variation is about +/- 0.03-0.05 in each band.

The data gap in Fig. 5 in year 2004 is due to the incompleteness of the MODIS dataset we acquired to date. The remaining gaps will be filled in upon completion of the MODIS land

Collection 5 reprocessing, which also generates the MODIS subsets for the AERONET sites for the ASRVN.

4.2 IBRF vs. NBRF

As discussed in section 3.4, the NBRF, which is retrieved from 16 days of measurements, may have a delayed response to surface changes. In contrast,,the IBRF, derived from the last day of measurements, tracks surface spectral changes immediately. This improvement in temporal sensitivity is sometimes achieved with compromised data quality.

Figure 6 shows a comparison of NBRF and IBRF for the GSFC site for the spring green-up period (days 95-122) of 2005. There is a 7-day gap in the AERONET records due to cloudiness after day 101. As a consequence, the NBRF and IBRF images show a noticeable color difference on day 108, representing a delayed response of the NBRF to surface change. With the accumulation of six additional measurements, the color of the NBRF and IBRF images become consistent again on day 117. The lag in NBRF depends on the number of available clear-skies measurements and the rate of surface change.

Note, however, that the brightness of the IBRF images in Fig. 6 vary with the view zenith angle. This occurs because the IBRF images are not normalized, whereas the NBRF images show a stable green-up trend as expected. This confirms that IBRF is more useful for detecting surface changes as well as effects of storms, fires, etc. The more stable NBRF is likely more suitable for process models, where the models may be sensitive to noise in input data fields.

4.3 NDVI

The Normalized Differential Vegetation Index (NDVI) is a commonly used parameter to characterize vegetation canopies. NDVI can be directly derived from the ASRVN BRF and albedo products. NDVI can be generated from different reflectance parameters, and its sensitivity to viewing geometry and atmospheric conditions can change accordingly. Figure 7 shows the NDVI time series for the "green" and "urban" pixels of the GSFC site as calculated from NBRF, surface albedo, IBRF (representing different forms of top-of-canopy NDVI) and from TOA reflectance. One can see that, in agreement with expectations, the variation of NDVI derived from NBRF and surface albedo is much smaller than that derived from IBRF and TOA reflectance. The NDVIs derived from the atmospherically corrected products (NBRF, albedo and IBRF) are also greater than the TOA NDVI. This is an expected since atmospheric correction tends to reduce the red band reflectance more than the NIR signal. Comparing the NDVIs derived from IBRF and NBRF, we find that the NBRF NDVI generally responds to the seasonal changes in a timely manner, except for a delay in a some cases which are usually related to a gap in the AERONET data.

4.4 MODIS Terra vs. Aqua

ASRVN creates a sensor-specific time series record of the surface reflectance over AERONET sites. Fig. 8 compares the NBRF time series for 1.5 years of the "bright pixel" of the Solar Village site. The NBRFs are very close to each other which suggests a good relative calibration between the MODIS Terra and Aqua instruments. Generally, cross-calibration of sensors flying in different orbits is a very difficult task. With the accumulation of a longer time record and sufficient global statistics, the ASRVN dataset may become a valuable source for the cross-calibration analysis of different sensors.

5. Discussion

To date, the ASRVN system has been used mainly as a prototype and to verify more manually-derived MODIS and MISR results reported elsewhere. In the near future, the National Polar Orbiting Environmental Satellite System (NPOESS) era will begin (~ 2013-2026), preceded immediately by the NPOESS Preparatory Project (NPP) mission (launch ~2010) [26] , 2008]. NPP data should initially overlap that of EOS Aqua as both are polar afternoon orbiters (1330 equator crossing). Plans are already underway to incorporate ASRVN into EOS-to-NPP/NPOESS data comparisons, as well as NPP/NPOESS product validation and long-term stability analysis.

Under NPP/NPOESS, the Visible Infrared Imaging Radiometer Suite (VIIRS) will replace MODIS and NOAA's Advanced Very High Resolution Radiometer (AVHRR) as the nation's wide-swath multispectral sensor. The 22-band VIIRS provides most of the spectral measurements and capabilities afforded by MODIS. VIIRS bands have a resolution of 375 m or 750 m, and therefore are highly compatible with the existing ASRVN framework.

VIIRS will provide source data for several relevant Environmental Data Records (EDRs; similar to MODIS L2 swath products), including AOT, instantaneous broadband albedo, and Enhanced Vegetation Index (EVI). The latter is a top-of-canopy 3-band deterministic parameter similar to NDVI. The NPOESS Program has rigorously defined accuracy and precision error specifications for each EDR. Surface spectral surface reflectance will also be produced and archived, although the Program considers this an Intermediate Product (IP). Among other things, the IP designation does not carry accuracy specifications.

NPOESS EDRs are primarily intended for operational users (e.g., weather forecasting), and thus ground processing will occur much more rapidly than for EOS. Most EDRs will be available within 30 minutes of observation. Under such conditions, maintaining constant product quality will be more challenging than for EOS. Unfortunately, because NPOESS is an operational program, validation resources will be significantly more limited than during the EOS era. Nevertheless, EDR validation is highly important, both for EDR users and to verify that EDRs meet contractual error specifications. Further, the complete NPOESS program will likely include three successive afternoon-overpass platforms (nominally launching in 2010 with NPP, 2013 and 2018). Relatively seamless EDR performance from platform to platform is critical for many users.

The NPOESS Land Validation Team, together with the prime NPOESS contractor, are responsible for assessing EDR accuracy. The Validation Team has identified AOT and Surface Reflectance as the highest priority land-related products for post-launch validation. Further, the Team has defined an initial strategy that strongly emphasizes the use of operational field network datasets (e.g., AERONET + ASRVN) over field campaigns. The Team is currently coordinating activities with the prime contractor, and we envision that, similar to MODIS, the operational processing center will generate EDR spatial subsets of relevant EDRs for ASRVN in near real time. Several targeted post-launch field campaigns will be undertaken to verify ASRVN results and document performance. NPOESS validation activities and resources are expected to decrease over time as the program focuses on long-term performance monitoring. ASRVN is expected to be critical resource throughout.

6. Concluding Remarks

This paper presented a new operational data collection and processing system ASRVN, which was initially designed for validation of the surface reflectance products. ASRVN collects MODIS and MISR L1B data for 50×50 km^2 areas for about 160 AERONET sites, and performs independent rigorous atmospheric correction using AERONET aerosol and column water vapor data. The atmospheric correction is achieved by fitting 16-day (multi-angle) sets of MODIS TOA measurements with theoretical reflectance accurately parameterized in terms of coefficients of the LSRT BRF model. The algorithm has a thorough data quality analysis component, including a cloud mask, an aerosol filter, and the control of the time series consistency of surface BRF and albedo.

The algorithm is optimized in terms of noise reduction and its ability to track both seasonal and rapid surface change. During stable surface conditions, such as periods of maximum greenness during summertime in the northern hemisphere, a 16-day BRF retrieval gives a solution characterized by low noise. When the surface changes rapidly (e.g., agricultural harvesting), the algorithm gives greater weight to the last MODIS measurement of the period thus quickly adjusts to the surface change.

We have also developed a back-up mechanism to cover extended periods of high cloudiness, when the number of cloud-free MODIS measurements in 16-day Queue is insufficient for the BRF retrieval. In this case, we use BRF scaling. This approach requires knowledge of the BRF shape which usually comes from the previous solution stored in the Q-memory. However, if there were no retrievals in the past 32 days, the algorithm substitutes the Q-solution with the historic seasonal BRF, which represents a quarterly-average BRF over years of retrievals. This method allows us to rapidly initialize retrievals after long periods of cloudiness and provide continuous gap-filled imagery of high quality.

The ASRVN suite of products includes three parameters of the LSRT model (k^L, k^G, k^V), surface spectral albedo, NBRF (a BRF value computed for a standard viewing geometry, VZA=0^o, SZA=45^o), and IBRF (a "scaled" BRF value derived from the last day of MODIS measurements at specific viewing geometry). All parameters are produced daily for seven 500 m MODIS bands at gridded 1 km resolution. We do not store vegetation indices like NDVI which are easy to produce from the available data.

The ASRVN dataset, including 6 years of MODIS TERRA and 1.5 years of MODIS AQUA data, is available for public download through LAADS website (Level 1 and atmosphere archive and Distribution System, http://ladsweb.nascom.nasa.gov/data/search.html). The products are accompanied by a Quality Assurance (QA) flag and color-composite RGB browse images for the TOA MODIS reflectance, NBRF, *IBRF*, cloud mask and QA.

The algorithm has high computational efficiency. For example, full ASRVN re-processing of 6 years of MODIS TERRA data at 100 AERONET sites takes about 24-30 hours using one processor of a 2.2 GHz workstation.

The results show very stable and reproducible NBRF and NDVI time series for any given pixel. The main source of errors in the developed algorithm is the variation of MODIS pixels with scan angle, which increase by a factor of eight from the nadir view to the edge of scan. This effect is partially mitigated by a 1 km resolution gridding procedure, but it is not cancelled entirely. In this regard, expansion of ASRVN with data from the future VIIRS instruments –

which features constrained pixel growth -- or geostationary sensors, such as the future GOES-R, is expected to produce a higher quality data set. Indeed, the NPOESS Land Product Validation Team's initial validation plan includes an AERONET+ASRVN component.

The ASRVN applications range from product validation and science analysis to sensor calibration support and long-term trending and stability studies. We believe the products from ASRVN fit well into the CEOS BELMANIP framework and will assist in more reliable and quantitative intercomparison analysis over the AERONET sites. Recently, we conducted a validation study of the MISR surface BRF and albedo products [10]. Because ASRVN produces a multi-year record for each sensor of interest, these data are useful for sensor cross-calibration analysis [27] and detection of long-term calibration trends. The latter are particularly important for climate applications.

Our approach can be considered as an indirect validation network for current MODIS or MISR surface reflectance and associated products (e.g., NDVI). If supported by periodic ground measurements over carefully selected stable homogenous test sites with different surface brightness level, which would establish an absolute reference for BRF and albedo, this approach can also be considered a full validation that is easily expandable to global level given the AERONET global infrastructure.

Acknowledgements. The work of Dr. Lyapustin and Dr. Wang was supported by the NASA EOS Science (Dr. D. Wickland) grant and NASA NPP (Dr. J. Gleason) grant.

APPENDIX

A-1. Parameterized expression for the TOA radiance

The algorithm is based on a high accuracy semi-analytical formula derived with the Green's function method [23, 28]. Below, τ is atmospheric optical thickness, πS_λ is spectral extraterrestrial solar irradiance, and $s=(\mu=\cos\theta,\ \varphi)$ is a vector of direction defined by zenith (θ) and azimuthal (φ) angles. The z-axis is pointed downwards, so $\mu_0>0$ for the solar beam and $\mu<0$ for the reflected beam. The TOA radiance $L(s_0,s)$ is expressed as a sum of the atmospheric path radiance (D), and surface-reflected radiance (L_s), directly and diffusely transmitted through the atmosphere:

$$L(s_0,s)=D(s_0,s)+L_s(s_0,s)e^{-\tau/|\mu|}+L_s^d(s_0,s)\,. \qquad \text{(A-1)}$$

The surface-reflected radiance is written as:

$$L_s(s_0,s)\cong S_\lambda\mu_0 e^{-\tau/\mu_0}\{\rho(s_0,s)+\alpha c_0\rho_1(\mu)\rho_2(\mu_0)\}+\frac{\alpha}{\pi}\int_{\Omega^+}D_s(s_0,s')\rho(s',s)\mu' ds'\,, \qquad \text{(A-2)}$$

where D_s is path radiance incident on the surface, c_0 is spherical albedo of the atmosphere, and

$$\rho_1(\mu)=\frac{1}{2\pi}\int_{\Omega^+}\rho(s',s)ds'\,,\ \rho_2(\mu_0)=\frac{1}{2\pi}\int_{\Omega^-}\rho(s_0,s)ds\,. \qquad \text{(A-3)}$$

α is a multiple reflection factor, $\alpha = (1 - q(\mu_0)c_0)^{-1}$, where q is surface albedo. The diffusely transmitted surface-reflected radiance at the TOA is calculated from L_s with the help of 1D diffuse Green's function of the atmosphere:

$$L_s^d(s_0, s) = \int_{\Omega^-} G^d(s_1, s) L_s(s_0, s_1) ds_1 . \quad \text{(A-4)}$$

The function πG^d is often called bi-directional upward diffuse transmittance of the atmosphere. The method of its calculation was discussed in detail in [23]. The surface albedo is defined as a ratio of reflected and incident radiative fluxes at the surface:

$$q(\mu_0) = F^{Up}(\mu_0) / F^{Down}(\mu_0), \quad \text{(A-5a)}$$

$$F^{Down}(\mu_0) = \pi S_\lambda \mu_0 e^{-\tau/\mu_0} + \int_{\Omega^+} D_s(s_0, s') \mu' ds' = F_s^{Dir}(\mu_0) + F_s^{Dif}(\mu_0), \quad \text{(A-5b)}$$

$$F^{Up}(\mu_0) = \pi S_\lambda \mu_0 e^{-\tau/\mu_0} q_2(\mu_0) + \int_{\Omega^+} \mu' q_2(\mu') D_s(s_0, s') ds', \; q_2(\mu_0) = \frac{1}{\pi} \int_{\Omega^-} \rho(s_0, s) \mu ds . \quad \text{(A-5c)}$$

These formulas give an explicit expression for the TOA radiance as a function of surface BRF. The accuracy of the above formulas is high, usually within a few tenths of a percent [23]. Below we will use the TOA reflectance, which is defined as

$$R_\lambda = L_\lambda / (\mu_0 S_\lambda) . \quad \text{(A-6)}$$

A-2. Expression for the TOA reflectance using *LSRT* BRF model

Based on the described semi-analytical solution, we can express TOA reflectance as an explicit function of parameters of the BRF model. We are using a semi-empirical Li Sparse – Ross Thick (LSRT) BRF model [29] as a basis. This is a linear model, represented as a sum of Lambertian, geometric-optical, and volume scattering components:

$$\rho(\mu_0, \mu, \varphi) = k^L + k^G f_G(\mu_0, \mu, \varphi) + k^V f_V(\mu_0, \mu, \varphi) . \quad \text{(A-7)}$$

It uses predefined geometric functions (kernels) f_G, f_V to describe different angular shapes. The kernels are independent of the land conditions. The BRF of a pixel is characterized by a combination of three kernel weights, $\vec{K} = \{k^L, k^G, k^V\}^T$. The LSRT model is used in the operational MODIS BRF/albedo algorithm [9].

The substitution of equation (A-7) into (A-1 - A-5), and normalization to the reflectance units gives the following expressions for the surface-reflected signal (the last two terms of Eq. (A-1)):

$$\begin{aligned} R_s(\mu_0, \mu, \varphi) = {} & e^{-\tau/\mu_0} \{ k^L + k^G f_G(\mu_0, \mu, \varphi) + k^V f_V(\mu_0, \mu, \varphi) + \alpha c_0 \rho_1(\mu) \; \rho_2(\mu_0) \} \\ & + \alpha \mu_0^{-1} \{ k^L E_0^d(\mu_0) + k^G D_G^1(\mu_0, \mu, \varphi) + k^V D_V^1(\mu_0, \mu, \varphi) \} , \end{aligned} \quad \text{(A-8)}$$

$$\begin{aligned} R_s^d(\mu_0, \mu, \varphi) = {} & e^{-\tau/\mu_0} \times \{ [k^L G^{av}(\mu) + k^G G_G^1(\mu_0, \mu, \varphi) + k^V G_V^1(\mu_0, \mu, \varphi)] + \\ & \alpha c_0 \, [k^L G^{av}(\mu) + k^G G_G^{11}(\mu) + k^V G_V^{11}(\mu)] \, \rho_2(\mu_0) \} \\ & + \alpha \mu_0^{-1} \{ k^L E_0^d(\mu_0) G^{av}(\mu) + k^G H_G^1(\mu_0, \mu, \varphi) + k^V H_V^1(\mu_0, \mu, \varphi) \} . \end{aligned} \quad \text{(A-9)}$$

The surface albedo is written as:

$$q(\mu_0) = E_0^{-1}(\mu_0)\,\{\mu_0 e^{-\tau/\mu_0}\, q_2(\mu_0) + k^L E_0^d(\mu_0) + k^G D_G^3(\mu_0) + k^V D_V^3(\mu_0)\}. \qquad \text{(A-10)}$$

Different functions of these equations represent different integrals of the incident path radiance (D_s) and atmospheric Green's function (G) with the BRF kernels. They were described in [28] along with the numerical calculation method. Below, we give only the integral expressions:

$$\rho_1(\mu) = k^L + k^G f_G^1(\mu) + k^V f_V^1(\mu), \qquad \text{(A-11)}$$

$$\rho_2(\mu_0) = k^L + k^G f_G^2(\mu_0) + k^V f_V^2(\mu_0), \qquad \text{(A-12)}$$

$$q_2(\mu_0) = k^L + k^G f_G^3(\mu_0) + k^V f_V^3(\mu_0), \qquad \text{(A-13)}$$

$$D_k^1(\mu_0, \mu, \varphi - \varphi_0) = \frac{1}{\pi}\int_0^1 \mu' d\mu' \int_0^{2\pi} d\varphi' D_s(\mu_0, \mu', \varphi' - \varphi_0)\, f_k(\mu', \mu, \varphi - \varphi'), \qquad \text{(A-14)}$$

$$D_k^3(\mu_0) = \frac{1}{\pi}\int_0^{2\pi} d\varphi' \int_0^1 \mu' f_k^3(\mu') D_s(\mu_0, \mu'; \varphi') d\mu', \qquad \text{(A-15)}$$

$$G^{av}(\mu) = \int_{-1}^0 d\mu_1 \int_0^{2\pi} G^d(\mu_1, \mu, \varphi - \varphi_1) d\varphi_1, \qquad \text{(A-16)}$$

$$G_k^{11}(\mu) = \int_{-1}^0 f_k^1(\mu_1) d\mu_1 \int_0^{2\pi} G^d(\mu_1, \mu, \varphi - \varphi_1) d\varphi_1, \qquad \text{(A-17)}$$

$$G_k^1(\mu_0, \mu, \varphi - \varphi_0) = \int_{-1}^0 d\mu_1 \int_0^{2\pi} G^d(\mu_1, \mu, \varphi - \varphi_1)\, f_k(\mu_0, \mu_1, \varphi_1 - \varphi_0) d\varphi_1, \qquad \text{(A-18)}$$

$$H_k^1(\mu_0, \mu, \varphi - \varphi_0) = \int_{-1}^0 d\mu_1 \int_0^{2\pi} G^d(\mu_1, \mu, \varphi - \varphi_1) D_k^1(\mu_0, \mu_1, \varphi_1 - \varphi_0) d\varphi_1. \qquad \text{(A-19)}$$

The subscript k in the above expressions refers to either geometric-optical (G) or volumetric (V) kernels, and the supplementary functions of the BRF kernels are given by:

$$f_k^1(\mu) = \frac{1}{2\pi}\int_0^1 d\mu' \int_0^{2\pi} f_k(\mu', \mu, \varphi' - \varphi) d\varphi', \qquad \text{(A-20a)}$$

$$f_k^2(\mu_0) = \frac{1}{2\pi}\int_{-1}^0 d\mu_1 \int_0^{2\pi} f_k(\mu_0, \mu_1, \varphi_1 - \varphi_0) d\varphi_1, \qquad \text{(A-20b)}$$

$$f_k^3(\mu') = \frac{1}{\pi}\int_{-1}^0 \mu d\mu \int_0^{2\pi} f_k(\mu', \mu, \varphi - \varphi') d\varphi. \qquad \text{(A-20c)}$$

The diffuse and total spectral surface irradiance are calculated from (A-5b) as:

$$E_0^d(\mu_0) = F^{Dif}(\mu_0)/(\pi S_\lambda),\ E_0(\mu_0) = F^{Down}(\mu_0)/(\pi S_\lambda). \qquad \text{(A-21)}$$

Let us re-write these equations separating the kernel weights. First, single-out small terms proportional to the product $c_0\rho_2(\mu_0)$ into the non-linear term:

$$R^{nl}(\mu_0, \mu) = \alpha c_0\, \rho_2(\mu_0)\, e^{-\tau/\mu_0}\,\{e^{-\tau/|\mu|}\, \rho_1(\mu) + k^L G^{av}(\mu) + k^G G_G^{11}(\mu) + k^V G_V^{11}(\mu)\}. \qquad \text{(A-22)}$$

Second, collect all remaining multiplicative factors for the kernel weights:

$$F^L(\mu_0,\mu) = (e^{-\tau/\mu_0} + \alpha\mu_0^{-1}E_0^d(\mu_0))(e^{-\tau/|\mu|} + G^{av}(\mu)), \quad \text{(A-23)}$$

$$F^k(\mu_0,\mu;\varphi) = \{e^{-\tau/\mu_0}\ f_k(\mu_0,\mu,\varphi) + \alpha\mu_0^{-1}D_k^1(\mu_0,\mu,\varphi)\}\, e^{-\tau/|\mu|} + e^{-\tau/\mu_0}\, G_k^1(\mu_0,\mu,\varphi) + \alpha\mu_0^{-1}H_k^1(\mu_0,\mu,\varphi),\ k=V, G. \quad \text{(A-24)}$$

With these notations, the TOA reflectance becomes:

$$R(\mu_0,\mu,\varphi) = R^D(\mu_0,\mu,\varphi) + k^L F^L(\mu_0,\mu) + k^G F^G(\mu_0,\mu,\varphi) + k^V F^V(\mu_0,\mu,\varphi) + R^{nl}(\mu_0,\mu). \quad \text{(A-25)}$$

This equation, representing TOA reflectance as an explicit function of the BRF model parameters, provides the means for an efficient atmospheric correction.

References

[1] M.King, & R.Greenstone, Eds., *EOS reference handbook: a guide to Earth ScienceEnterprise and the Earth Observong System*. Greenbelt, MD: EOS Project Science Office, NASA/Goddard Space Flight Center, 1999, p. 355.

[2] Morisette, J. T., J. L. Privette, C. O. Justice, A framework for the validation of MODIS land products. *Remote Sens. Environ*., **83**, pp. 77-96, 2002.

[3] Wang, Y., Woodcock, C. E., Buermann, W., Stenberg, P., Voipio, P., Smolander, H., Häme, T., Tian, Y., Hu, J., Knyazikhin, Y. and Myneni, R. B. (2004), Evaluation of the MODIS LAI algorithm at a coniferous forest site in Finland, *Remote Sens. Environ*., 91:114-127.

[4] Tian, Y., Woodcock, C. E., Wang, Y., Privette, J. L., Shabanov, N. V., Zhou, L., Buermann, W., Dong, J., Veikkanen, B., Hame, T., Ozdogan M., Knyazikhin Y., and Myneni, R. B., (2002), Multiscale Analysis and Validation of the MODIS LAI Product over Maun, Botswana, I. uncertainty assessment, *Remote Sens. Environ.*, 83:414-430.

[5] Tian, Y., Woodcock, C. E., Wang, Y., Privette, J. L., Shabanov, N. V., Zhou, L., Buermann, W., Dong, J., Veikkanen, B., Hame, T., Ozdogan M., Knyazikhin Y., and Myneni, R. B., (2002), Multiscale Analysis and Validation of the MODIS LAI Product over Maun, Botswana, II. Sampling strategy, *Remote Sens. Environ*., 83:431-441.

[6] Garrigues, S, Lacaze R, Baret F, Morisette JT, Weiss M, Nickeson JE, Fernandes R, Plummer S., Shabanov NV, Myneni RB, Knyazikhin Y, and Yang W, (2008).Validation and Intercomparison of Global Leaf Area Index Products Derived From Remote Sensing Data, *J. Geophys. Res*., in press.

[7] Baret, F., J. Morisette, R. Fernandes, J.L. Champeaux, R. Myneni, J. Chen, S. Plummer, M. Weiss, C. Bacour, G.Derive, (2006), Evaluation of the representativeness of networks of sites for the validation and inter-comparison of global land biophysical products. Proposition of the CEOS-BELMANIP, *IEEE Trans. Geosci. Remote Sens*., 44(7)1794-1803.

[8] Holben, B. N., T. F. Eck, I. Slutsker, D. Tanré, J. P. Buis, A. Setzer, E. Vermote, J. A. Reagan, Y. J. Kaufman, T. Nakajima , F. Lavenu, I. Jankowiak, A. Smirnov, AERONET-A Federated Instrument Network and Data Archive for Aerosol Characterization, *Rem. Sens. Environ.*, **66,** 1-16, 1998.

[9] Schaaf, C. B., F. Gao, A. H. Strahler, W. Lucht, X. Li, T. Tsang, N. C. Strugnell, X. Zhang, Y. Jin, J.-P. Muller, P. Lewis, M. Barnsley, P. Hobson, M. Disney, G. Roberts, M. Dunderdale, C. Doll, R. d'Entremont, B. Hu, S. Liang, and J. L. Privette, (2002), First

Operational BRDF, Albedo and Nadir Reflectance Products from MODIS, *Remote Sens. Environ.*, 83, 135-148.

[10] Lyapustin, A., Wang, Y., J. Martonchik, Privette, J., Holben, B., Slutsker, I., Sinyuk, A., Smirnov, A., (2006), Local Analysis of MISR Surface BRF and Albedo Over GSFC and Mongu AERONET Sites, *IEEE Trans. Geosci. Remote Sens.*, 44:1707-1718.

[11] Dubovik, O., M. D. King, A flexible inversion algorithm for retrieval of aerosol optical properties from Sun and sky radiance measurements, *J. Geophys. Res.*, **105**, 20,673-20,696, 2000.

[12] Dubovik, O., B. Holben, T. F. Eck., A. Smirnov, Y. J. Kaufman, M. D. King, D. Tanre, and I. Slutzker, Variability of absorption and optical properties of key aerosol types observed in worldwide locations, *J. Atmos. Sci.*, **59**, 590-608, 2002.

[13] O. Dubovik, A. Sinyuk, T. Lapyonok, B. N. Holben, M. Mishchenko, P. Yang, T. F. Eck, H. Volten, O.Munoz, B. Veihelmann, W. J. van der Zande, J. Leon, M. Sorokin, and I. Slutsker, "Application of spheroid models to account for aerosol particle nonsphericity in remote sensing of desert dust", *J .Geophys. Res.*, vol. 111, D11208, doi:10.1029/2005JD006619, 2006.

[14] Dubovik, O., A. Smirnov, B. N. Holben, M. D. King, Y. J. Kaufman, T. F. Eck, and I. Slutsker: Accuracy assessments of aerosol optical properties retrieved from AERONET sun and sky-radiance measurements, *J.Geophys. Res.*, **105**, 9791-9806, 2000.

[15] Lyapustin, A. I., and T. Z. Muldashev, Method of spherical harmonics in the radiative transfer problem with non-Lambertian surface, *J. Quant. Spectrosc. Radiat. Transfer*, **61**, 545-555, 1999.

[16] Lyapustin, A., 2003: Interpolation and Profile Correction (IPC) method for shortwave radiative transfer in spectral intervals of gaseous absorption. *J. Atmos. Sci.*, **60**, 865-871.

[17] Wolfe, R. E., Roy, D. P., and Vermote, E. (1998). MODIS Land Data Storage, Gridding, and Compositing Methodology: Level 2 Grid. *IEEE Trans. Geosci. Remote Sens.*, 36, 1324–1338.

[18] Smirnov A., B.N. Holben, T.F. Eck, O. Dubovik, and I. Slutsker, Cloud screening and quality control algorithms for the AERONET data base, *Rem.Sens.Env., 73*, 337-349, 2000.

[19] Lyapustin, A., Y. Wang, and R. Frey, "An Automatic Cloud Mask Algorithm Based on Time Series of MODIS Measurements", *J. Geophys. Res.*, in press.

[20] X. Li and A. H. Strahler, "Geometric-optical bidirectional reflectance modeling of the discrete crown vegetation canopy: Effect of crown shape and mutual shadowing", *IEEE Trans. Geosci. Remote Sens.*, vol. 30, pp. 276-292, 1992.

[21] Vermote, E.F., A. Vermeulen, 1999. Atmospheric correction algorithm: spectral reflectances (MOD09). Algorithm theoretical basis document. NASA EOS-MODIS Doc., Version 4.0, 107 pp.

[22] Lyapustin, A. I., Atmospheric and geometrical effects on land surface albedo, *J. Geophys. Res.*, **104**, 4123-4143, 1999.

[23] Lyapustin, A., and Yu. Knyazikhin, Green's function method in the radiative transfer problem. I: Homogeneous non-Lambertian surface, Appl. Optics, 40, 3495-3501, 2001.

[24] Lyapustin, A., and Yu. Knyazikhin, Green's function method in the radiative transfer problem. II: Spatially heterogeneous anisotropic surface, Appl. Optics, 41, 5600-5606, 2002.

[25] Strugnell, N., and W. Lucht, An algorithm to infer continental-scale albedo from AVHRR data, land cover class and field observations of typical BRDFs, J. Climate, 14, 1360-1376, 2001.
[26] Justice C.O., Vermote E., J. Privette and A. Sei (2008), The Evolution of U.S. Moderate Resolution Optical Moderate Resolution Land Remote Sensing from AVHRR to MODIS to VIIRS, chapter in *Land Remote Sensing and Global Environmental Change: NASA's EOS and the Science of ASTER and MODIS*, submitted
[27] Lyapustin, A., Y. Wang, R. Kahn, J. Xiong, A. Ignatov, R. Wolfe, A. Wu, B. Holben, C. Bruegge, 2007: Analysis of MODIS-MISR calibration differences using surface albedo around AERONET sites and cloud reflectance. Rem. Sens. Environment, 107, 12-21.
[28] Lyapustin, A., and Y. Wang, (2005), Parameterized Code Sharm-3D for Radiative Transfer Over Inhomogeneous Surfaces, *Appl. Optics*, **44**, 7602-7610.
[29] Lucht W., Schaaf C. B., Strahler A. H., (2000), An algorithm for the retrieval of albedo from space using semiempirical BRDF models , *IEEE Trans. Geosci. Remote Sens.*, **38**, 977-998.

Table 1. ASRVN product suite

Product Name	Data Type	Dimensions	Descriptions	MODIS Product Counterpart
CloudMask	DFNT_UINT8	50x50	Cloud mask field, the definition of values is shown in Table 2.	MOD35 cloud Mask
NBRF	DFNT_FLOAT32	50x50x7	Bi-directional reflectance function normalized to SZA=45^o and nadir view.	MOD43B4 Nadir BRDF-Adjusted Reflectance (NBAR)
Albedo	DFNT_FLOAT32	50x50x7	Surface albedo at a given solar zenith angle in ambient atmospheric conditions.	A combination of MOD43B3 black-sky and white-sky albedo weighted with respective relative direct and diffuse incident fluxes.
IBRF	DFNT_FLOAT32	50x50x7	Instantaneous (or one-angle) BRF for specific viewing geometry of the last day of observations.	MOD09 Surface reflectance
Kiso	DFNT_FLOAT32	50x50x7	BRF model parameter, the isotropic coefficient.	MOD43B1 BRDF/Albedo Model Parameters
Kvol	DFNT_FLOAT32	50x50x7	BRF model parameter, the volumetric coefficient.	MOD43B1 BRDF/Albedo Model Parameters
Kgeo	DFNT_FLOAT32	50x50x7	BRF model parameter, the geometric-optics coefficient.	MOD43B1 BRDF/Albedo Model Parameters
QA	DFNT_UINT16	50x50	Quality assurance flags. The definition of each field can be found in Table 3.	N/A
RGB browse image	N/A	50x50	The RGB browse image including TOA reflectance, NBRF, IBRF, CM and QA.	N/A

Table 2. Cloud mask field definition

Value	Definition
1	Clear
2	Possibly clear
3	Possibly cloudy
4	Cloudy
5	Cloud shadow
6	“grey” area around cloud pixel, or inhomogeneous aerosol.
10	Clear water
11	Clear snow
12	Clear Land (equivalent to 1)
13	Clear water (equivalent to 10)

Table 3. QA field definition

Bit field	Bits	Range	Bit-code definition
QA.overall	0-1	00-11	00 – Good quality 01 – acceptable quality 10 – BRF parameters and NBRF are filled with previous results, IBRF is not created 11 – No result is created
QA.scale	2	0-1	0 – Not scaled 1 – scaled
QA.nDelay	3-7	0-31	The number of days since last update of Q-memory
QA.status	8-9	00-11	00 – the BRF consistency parameter *status* =0 01 – *status* =1 10 – *status* =2 11 – *status* >2 (reliable solution)
QA.adjCloud	10	0-1	0 – no adjacent cloud 1 – this pixel is adjacent to a cloudy pixel
QA.model	11	0-1	0 – the calculated IBRF is consistent with the model prediction 1 – the calculated IBRF is not consistent with the model prediction
QA.cloud	12	0-1	0 – the pixel is clear 1 – the pixel is cloudy

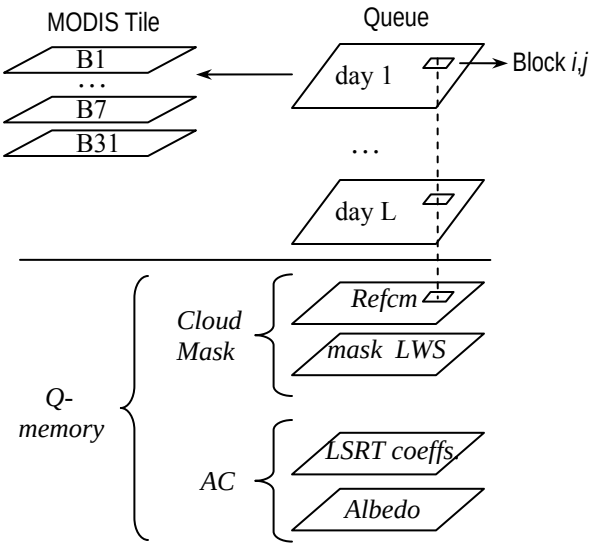

Figure 1. Structure of Queue for *ASRVN* processing. The Queue, designed for the sliding window algorithm, stores up to 16 days of gridded MODIS observations at 1 km resolution. The CM algorithm uses MODIS bands 1-7 and band 31, which are stored as Layers (double-indexed arrays) shown in the upper-left corner. A dedicated Q-memory is allocated to store the ancillary information for CM algorithm in *Refcm* structure, such as a reference clear-skies image (*refcm*) and results of dynamic Land-Water-Snow classification (*mask_LWS*). This information is updated with latest measurements (day L) once given block is found cloud-free, thus adapting to changing surface conditions. The Q-memory also stores results of previous reliable BRF retrievals, or atmospheric correction (AC), for MODIS bands 1-7.

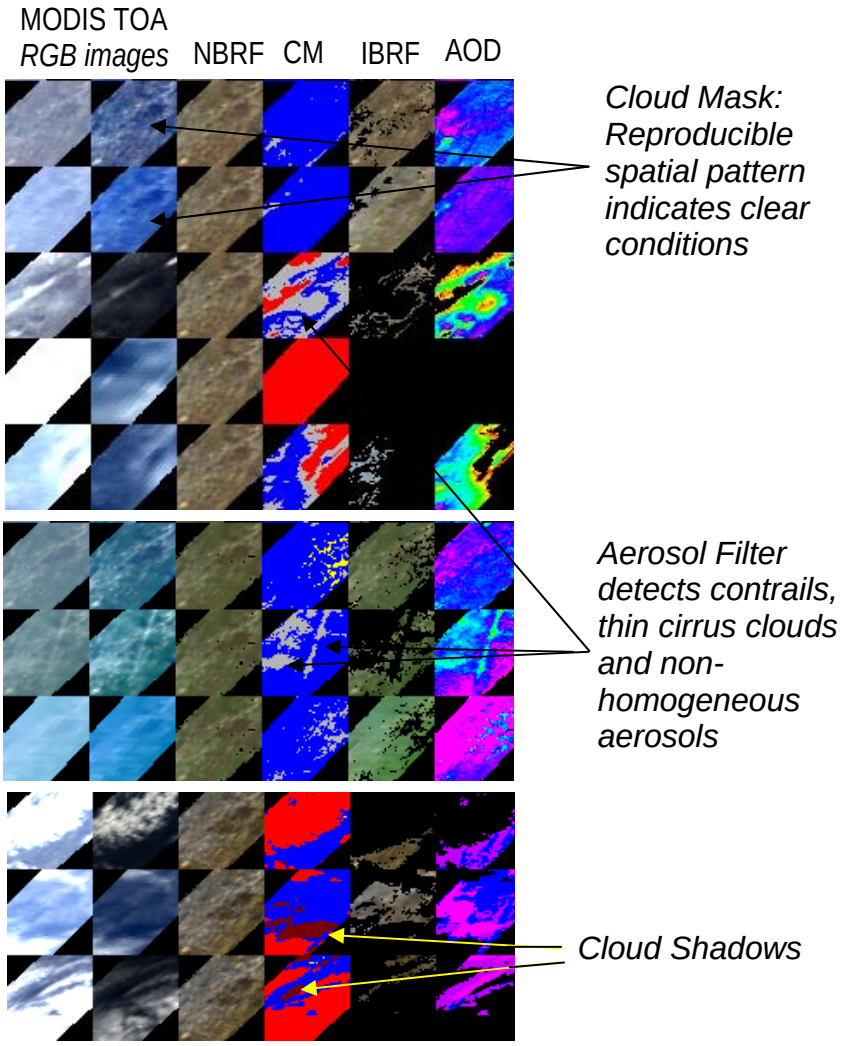

Figure 2. Example of ASRVN processing for GSFC, USA, 2006. The two left columns show the top-of-atmosphere (TOA) gridded RGB MODIS TERRA images for three different sequences of observations. The two left images are differently normalized to help distinguish clouds. The fourth column shows the total generated cloud mask (CM legend: clear – blue, cloud – red, possibly cloud – yellow, cloud shadow – dark red, aerosol filter – grey). The last column shows the aerosol optical depth (AOD) retrieved from the last day of measurement, which is used in aerosol filter. The third and fifth columns show the results of ASRVN atmospheric correction (see sec. 3.3).

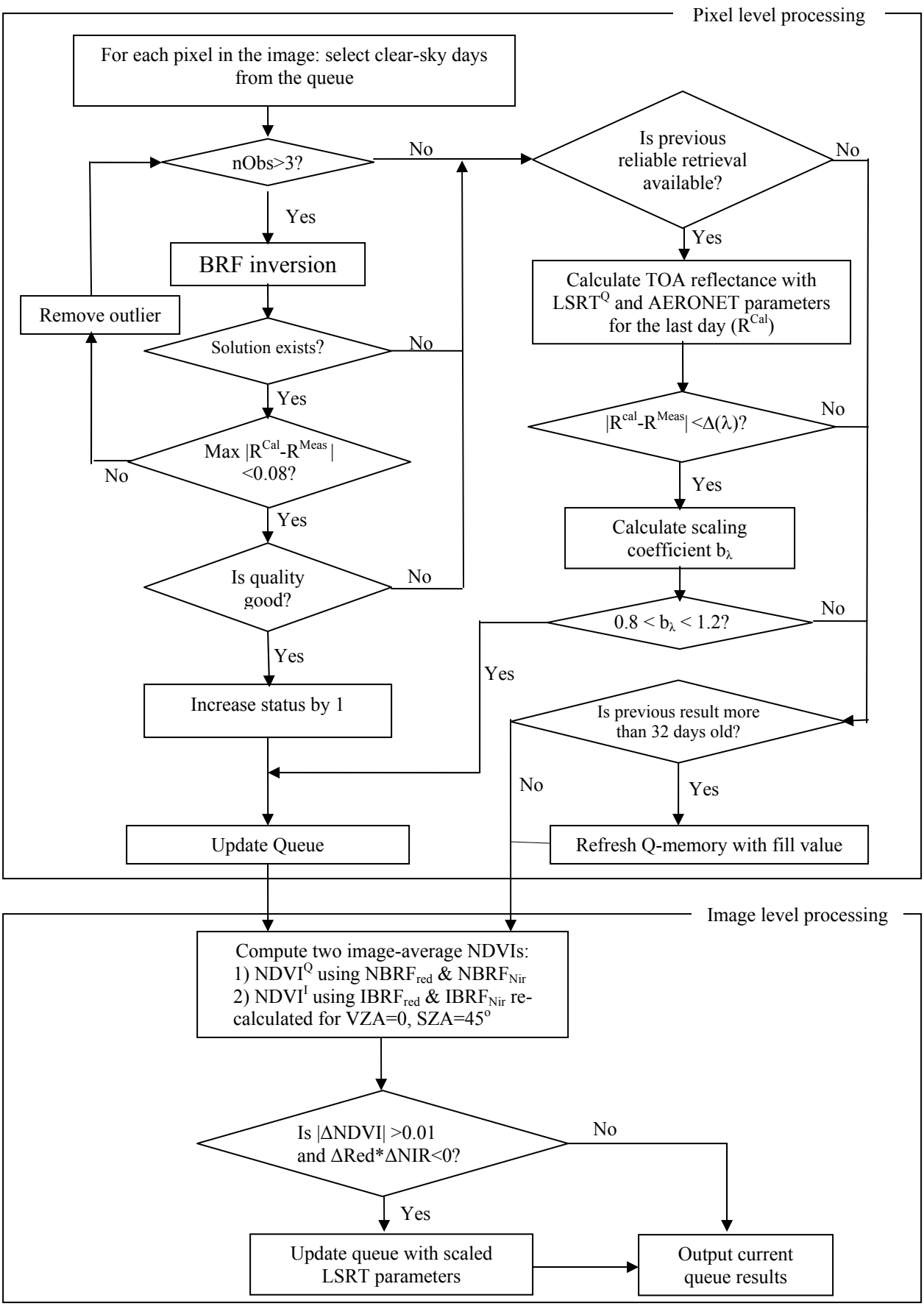
Pixel level processing
For each pixel in the image: select clear-sky days from the queue
nObs>3?
No
Yes
BRF inversion
Remove outlier
Solution exists?
No
Yes
Max |R^Cal-R^Meas| <0.08?
No
Yes
Is quality good?
No
Yes
Increase status by 1
Update Queue
Is previous reliable retrieval available?
No
Yes
Calculate TOA reflectance with LSRT^Q and AERONET parameters for the last day (R^Cal)
|R^cal-R^Meas| <Δ(λ)?
No
Yes
Calculate scaling coefficient b_λ
0.8 < b_λ < 1.2?
No
Yes
Is previous result more than 32 days old?
No
Yes
Refresh Q-memory with fill value
Image level processing
Compute two image-average NDVIs:
1) NDVI^Q using NBRF_red & NBRF_Nir
2) NDVI^I using IBRF_red & IBRF_Nir re-calculated for VZA=0, SZA=45^o
Is |ΔNDVI| >0.01 and ΔRed*ΔNIR<0?
No
Yes
Update queue with scaled LSRT parameters
Output current queue results

Figure 3. Block-diagram of MODIS AC algorithm.

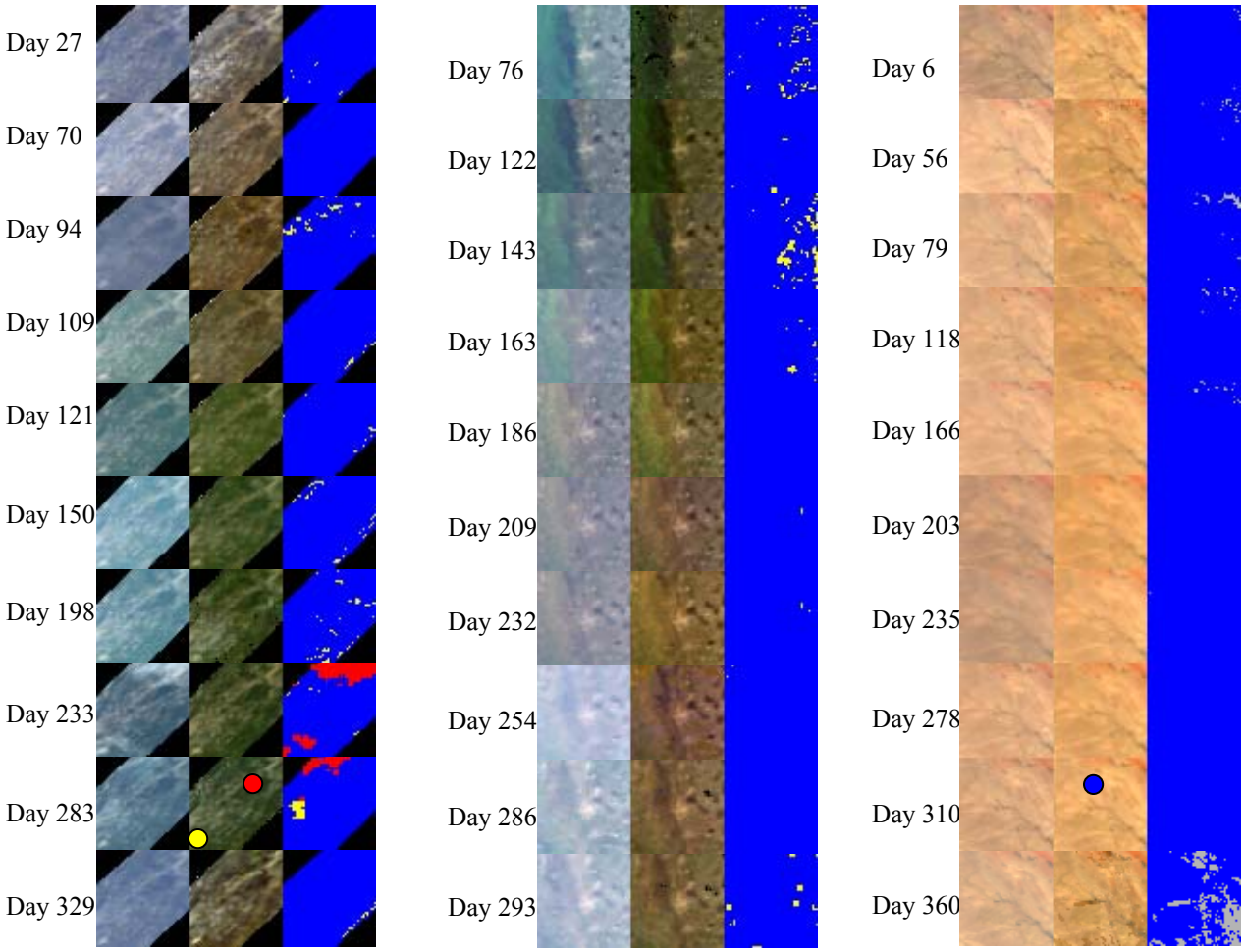

(a) (b) (c)

Figure 4. . Temporal dynamics of surface NBRF for a) GSFC in year 2005; b) Mongu site in year 2005 and c) Solar-village site in year 2006. They shown from left to right the RGB TOA MODIS gridded images, the RGB NBRF images and the cloud masks. The true color images are composed from equally weighted red, green and blue bands. . The CM legend is the same as in Figure 2. The red, yellow and blue dots in panel a) and c) show the location of selected "green" pixel, "urban" pixel and "bright" pixel, respectively.

a)

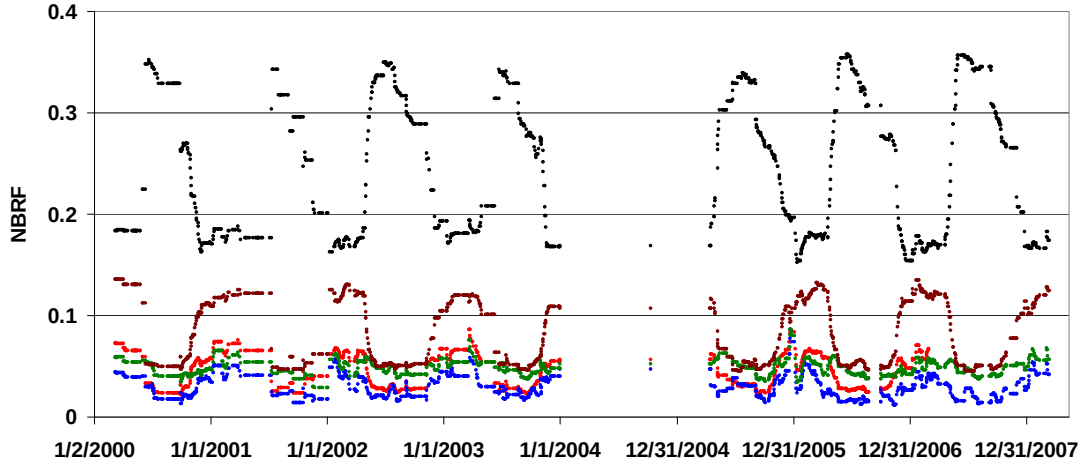
NBRF
0.4
0.3
0.2
0.1
0
1/2/2000
1/1/2001
1/1/2002
1/1/2003
1/1/2004
12/31/2004
12/31/2005
12/31/2006
12/31/2007

b)

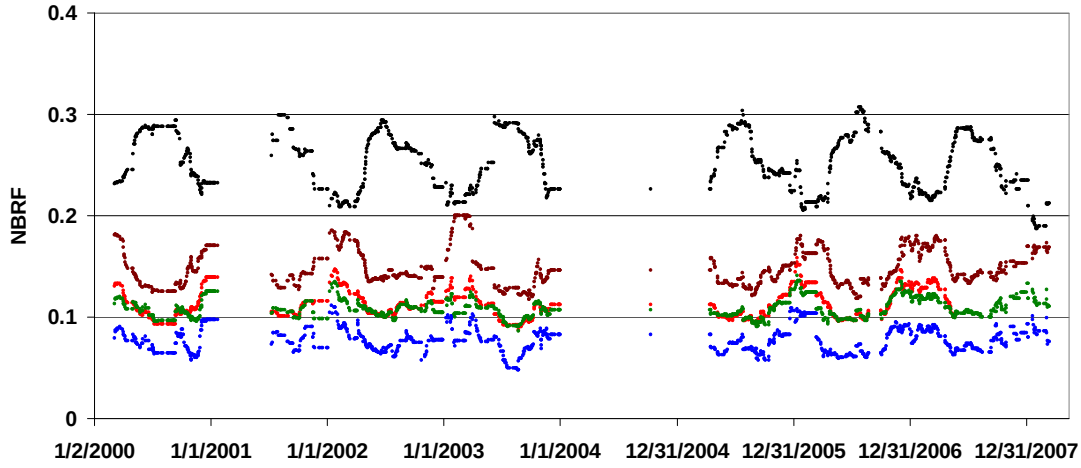
NBRF
0.4
0.3
0.2
0.1
0
1/2/2000
1/1/2001
1/1/2002
1/1/2003
1/1/2004
12/31/2004
12/31/2005
12/31/2006
12/31/2007

c)

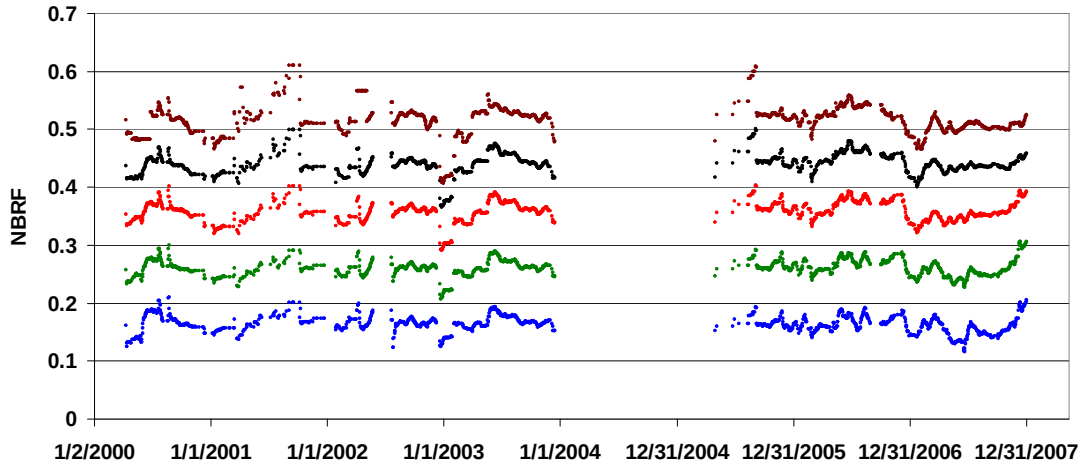
NBRF
0.7
0.6
0.5
0.4
0.3
0.2
0.1
0
1/2/2000
1/1/2001
1/1/2002
1/1/2003
1/1/2004
12/31/2004
12/31/2005
12/31/2006
12/31/2007

Figure 4. NBRF time series for a) green pixel, GSFC site; b) urban pixel, GSFC site and c) bright pixel, Solar village site. R, G, B color represents red, green and blue bands, respectively; black is NIR band and brown is band 7 (2.1μm).

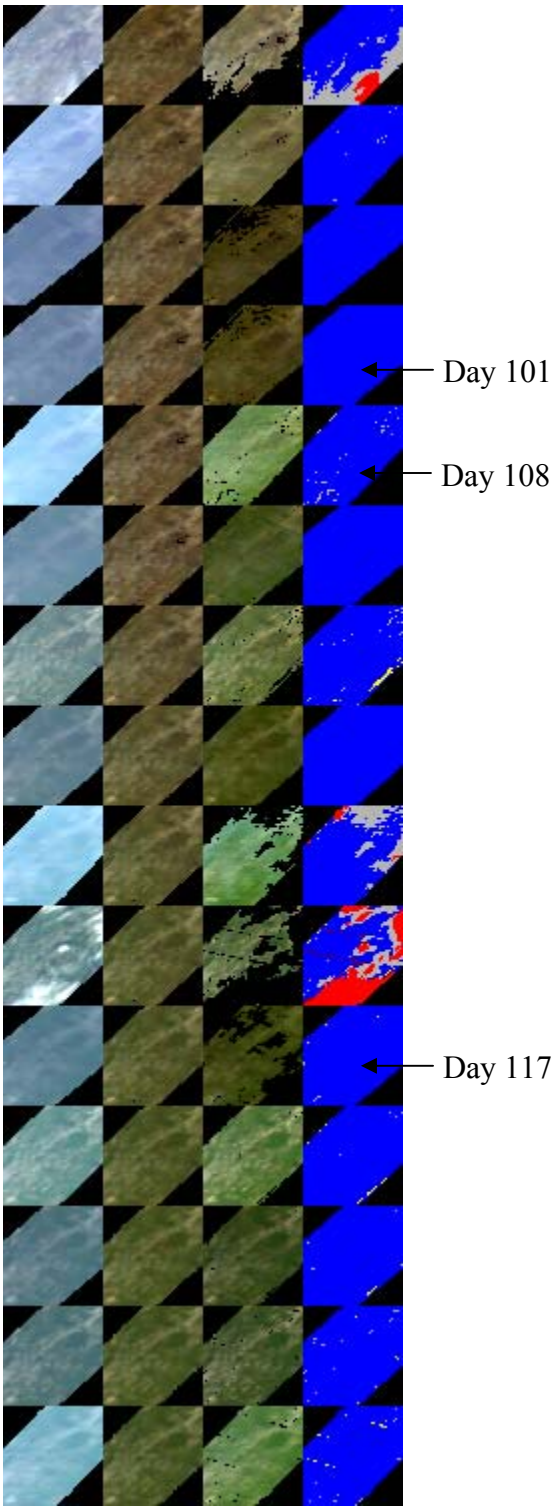

Figure 6. Comparison of NBRF and IBRF for GSFC, USA, day 95-122, 2006. Images shown from left to right are: RGB TOA MODIS gridded images, RGB NBRF images, RBG IBRF images and cloud mask. The CM legend is the same as in Figure 5.

a)

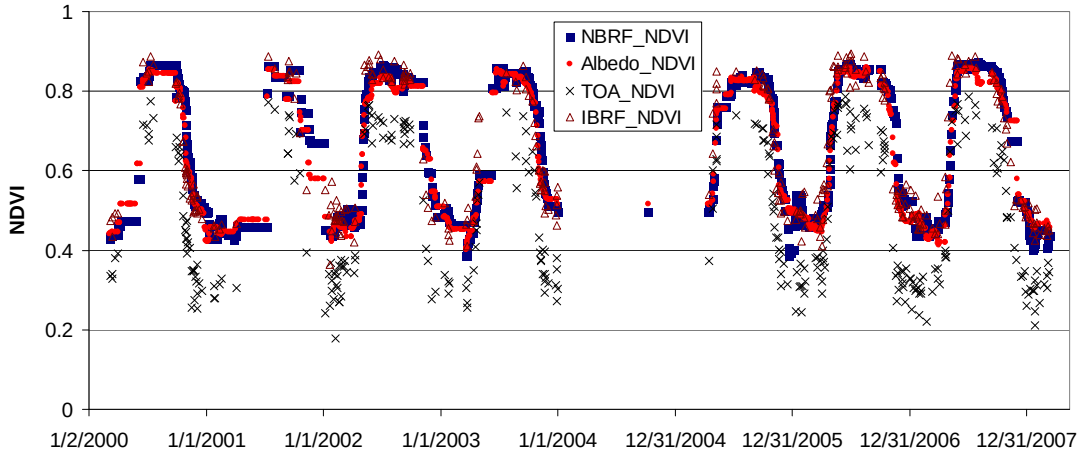

b)

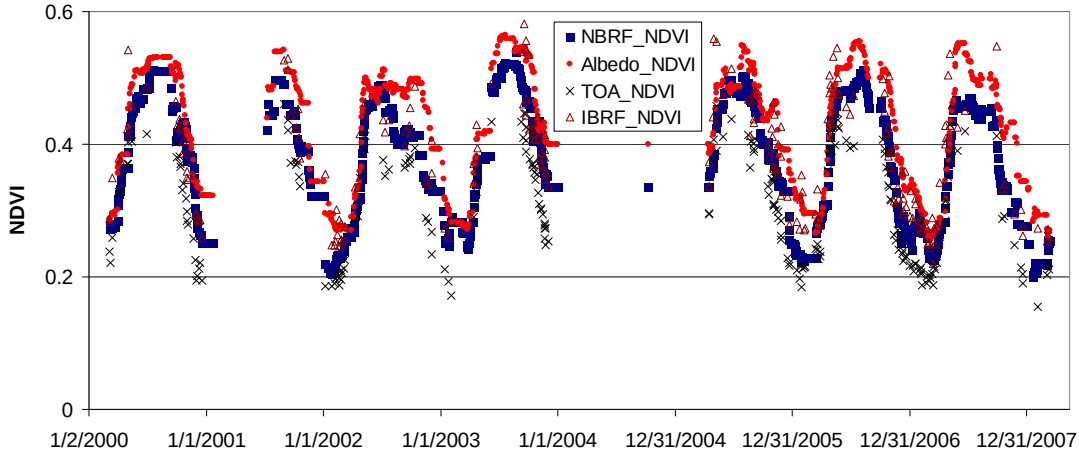

Figure 7. NDVI time series of a) “green pixel” and b) “urban” pixel in GSFC site.

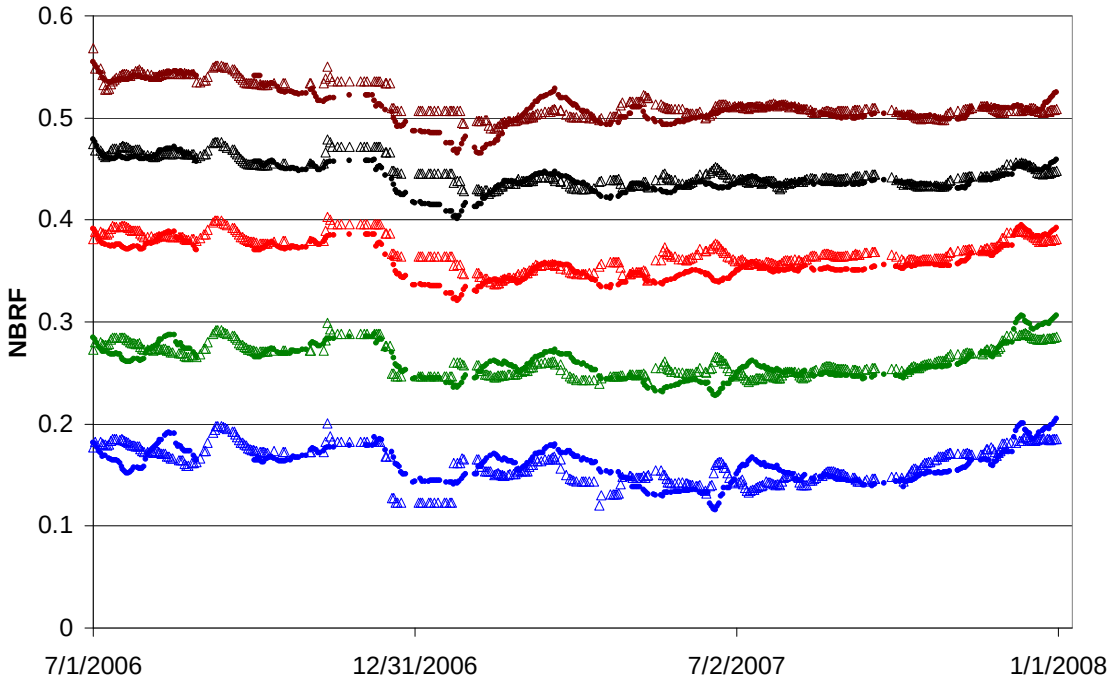

Figure 8. Comparison of MODIS Terra and Aqua NBRF for a bright pixel (Solar Village). Here, triangles and solid circles represent Aqua and Terra NBRF, respectively. Red, green and blue bands are shown with their respective color, black shows NIR band and brown corresponds to band 7 (2.1μm).